Available online at www.sciencedirect.com
SCIENCE DIRECT®
Acta Materialia 52 (2004) 4479–4492
Acta MATERIALIA
www.actamat-journals.com

On the lattice parameters of phases in binary Ti–Ni shape memory alloys

S.D. Prokoshkin [a,1], A.V. Korotitskiy [a,1], V. Brailovski [b,*], S. Turenne [c], I.Yu. Khmelevskaya [a,1], I.B. Trubitsyna [a,1]

[a] *Laboratory of Thermomechanical Treatment, Moscow Steel and Alloys Institute, Leninskiy Prosp. 4, Moscow 119049, Russia*
[b] *Mechanical Engineering Department, Ecole de Technologie Superieure, 1100 Notre-Dame Street West, Montreal, Que., Canada H3C 1K3*
[c] *Mechanical Engineering Department, Ecole Polytechnique de Montreal, P.O. Box 6079, Station Centre-Ville, Montreal, Que., Canada H3C 3A7*

Received 25 February 2004; received in revised form 12 May 2004; accepted 2 June 2004
Available online 15 July 2004

Abstract

An X-ray diffractometry study of Ti–47.0 to 50.7 at.%Ni alloys was performed. In the 50.0–50.7 at.% range of nickel content, a concentration dependence of B19′-martensite lattice parameters (MLP) is observed. MLP are found to be identical for 47.0 and 50.0 at.% of nickel content. The temperature dependence of MLP is observed, and this dependence is enhanced in the reverse transformation temperature range for Ti–50.0 at.%Ni alloy. MLP are different for the quenched martensite and for the martensite formed from the austenite containing a well-developed dislocation substructure. It is proven that the presence of an intermediate R-phase during martensitic transformation is not responsible for the changes in MLP, observed in hyper-equiatomic alloys or in alloys having a highly dislocated austenite substructure. In the 50.0 at.%Ni alloy, no changes in MLP are observed after a 25% cold-deformation of the already formed thermal martensite.

Keywords: Shape memory alloys; X-ray diffraction; Crystal structure; Lattice parameters

1. Introduction

Crystal lattice parameters of the high-temperature phase (austenite) and the low-temperature phase (martensite) are the basic characteristics of shape memory alloys because the level of the transformation lattice strain generated during austenite–martensite transformation determines a maximum resource for recovery strain. In binary Ti–Ni alloys, the crystal lattice of the martensite formed either directly from B2-austenite, or through an intermediate rhombohedral R-phase, represents the B19′-type monoclinic lattice [1–12]. The alloying of Ti–Ni alloys by a third element (Fe, Co, Cu, Au, Al, Mn, Pd, etc.) changes B19′-martensite lattice parameters and temperature ranges of transformations, and can lead to a separation of the B2-austenite transformations into R- or B19′-phases as intermediate and final phases of the martensite formation [10,13]. While the influence of alloying elements in ternary Ti–Ni-based alloys on the B19′-martensite lattice parameters (MLP) has been studied quite extensively [10,13], the nickel-concentration dependence of the B19′-MLP in binary Ti–Ni alloys remains questionable. To the best of the authors' knowledge, the published results on B19′-MLP measurement in binary Ti–Ni alloys ([1–12,14–16], Table 1) can be summarized as follows:

1. In the majority of investigations, the MLP are measured for a single alloy, which mainly has a near-equiatomic or pre-equiatomic (in nickel) nominal composition. A broad scattering in these results between various investigators does not allow a clear judgment about the MLP variations with

* Corresponding author. Tel.: +1-514-396-8594; fax: +1-514-396-8530.
E-mail addresses: prokoshkin@tmo.misis.ru (S.D. Prokoshkin), akorotitskiy@fromru.com (A.V. Korotitskiy), vbrailovski@mec.ets-mtl.ca (V. Brailovski).
[1] Tel.: +7-095-230-4405; fax: +7-095-247-6001.

1359-6454/$30.00 © 2004 Acta Materialia Inc. Published by Elsevier Ltd. All rights reserved.
doi:10.1016/j.actamat.2004.06.007

Table 1
19′-Martensite lattice parameters in Ti–Ni binary SMA from references

at.%Ni (nominal)	Treatment	M_S/T_R (°C)	Recording temperature (°C)		B19′-martensite lattice parameters					Note
					a (nm)	b (nm)	c (nm)	β (°)		
49.75	Aging	20/45	23 (reheating)		0.2870 ± 0.0010	0.4110 ± 0.0030	0.4600 ± 0.0030	97.4 ± 0.4		Caculated using d_{hkl} from [1]
50.0	Aging 450 °C, 48 h	90	20		0.2904 ± 0.0005	0.4121 ± 0.0002	0.4649 ± 0.0006	97.9 ± 0.1		Caculated using d_{hkl} from [2]
49.75	Quenching 1000 °C, 1 h	−40 to −50	−192		0.2889 ± 0.0005	0.4120 ± 0.0012	0.4622 ± 0.0016	96.8 ± 0.32		Taken from [3] $\sum(2\vartheta^{obs}_{hkl} - 2\vartheta^{cal}_{hkl})^2 = 0.096$ deg^2
					0.2874 ± 0.0006	0.4113 ± 0.0009	0.4630 ± 0.0009	97.0 ± 0.1		Caculated using d_{hkl} from [3] $\sum(2\vartheta^{obs}_{hkl} - 2\vartheta^{cal}_{hkl})^2 = 0.026$ deg^2
49.75	Quenching 1000 °C, 1 h	−40 to −50	−53		0.2880 ± 0.0005	0.4148 ± 0.0002	0.4621 ± 0.0003	96.4 ± 0.1		Caculated using ϑ_{hkl} from [4]
			−178		0.2872 ± 0.0003	0.4124 ± 0.0002	0.4632 ± 0.0003	96.9 ± 0.1		
50.5					0.2883	0.4117	0.4623	96.8		Taken from [5]
50.0	Cold rolling $\varepsilon = 30\%$	35	RT		0.2909 ± 0.0007	0.4141 ± 0.0003	0.4639 ± 0.0005	96.8 ± 0.2		Caculated using d_{hkl} from [6]
49.8	Aging 800 °C, 1 h	85	RT	B19′$_1$	0.2893	0.4120	0.4657	97.6	B19′$_1$	Taken from [7,14]
50.0		35/10								
50.3		30/10		B19′$_2$	∼0.2889	∼0.412	∼0.4622	∼96.8	B19′$_2$	
50.75		0/10								
50.0					0.2885	0.4120	0.4622	96.8		Taken from [8]
49.2	Quenching from 1000 °C, 1 h	50	RT		0.2898	0.4108	0.4646	97.78		Taken from [9]
48.5			20		0.290	0.411	0.466	97.8		Taken from [10]
50.0			20		0.289	0.412	0.464	97.3		
50.5			−50		0.289	0.415	0.464	97.1		
51.0			−150		0.289	0.414	0.465	97.1		
50.1	Aging 800 °C, 1 h	55/48	21		0.2896 ± 0.0006	0.4120 ± 0.0008	0.4640 ± 0.0009	97.2		Taken from [11] $\sum(2\vartheta^{obs}_{hkl} - 2\vartheta^{cal}_{hkl})^2 = 0.136$ deg^2
					0.2904 ± 0.0004	0.4141 ± 0.0003	0.4654 ± 0.0003	97.1 ± 0.1		Caculated using d_{hkl} from [11] $\sum(2\vartheta^{obs}_{hkl} - 2\vartheta^{cal}_{hkl})^2 = 0.002$ deg^2
			74		0.2893 ± 0.0003	0.4136 ± 0.0008	0.4629 ± 0.0009	96.8		Taken from [11] $\sum(2\vartheta^{obs}_{hkl} - 2\vartheta^{cal}_{hkl})^2 = 0.110$ deg^2
					0.2902 ± 0.0006	0.4155 ± 0.0003	0.4632 ± 0.0003	96.6 ± 0.1		Caculated using d_{hkl} from [11] $\sum(2\vartheta^{obs}_{hkl} - 2\vartheta^{cal}_{hkl})^2 = 0.005$ deg^2

50.5	Quenching 800 °C	⩽10	RT (reheating)	0.2886 ± 0.0003	0.4138 ± 0.0002	0.4629 ± 0.0002	96.7 ± 0.1	Calculated using d_{hkl} from [12]
			−20 (reheating)	0.2883 ± 0.0003	0.4132 ± 0.0003	0.4636 ± 0.0003	96.9 ± 0.1	
51.0	Aging 800 °C	~−50	−45	0.2887 ± 0.0003	0.4144 ± 0.0003	0.4634 ± 0.0002	96.7 ± 0.1	Calculated using ϑ_{hkl} from [15]
			−150	0.2898 ± 0.0004	0.4143 ± 0.0002	0.4653 ± 0.0003	97.3 ± 0.1	
50.5	Drawing + quenching from 500 °C	−10/22	−71	0.28815	0.41232	0.46256	97.0	Taken from [16]

nickel-concentration. Furthermore, in some works (for example [1,3,4]), the nominal nickel content in studied alloys does not correlate with the position of their M_S temperatures (the latter is determined by a real nickel content in solid solution [17–19]). As a result, a correlation analysis of MLP dependencies on the nominal nickel content with the Table 1 data gives very low correlation coefficients: $R_a = 0.08$, $R_b = 0.52$, $R_c = 0.13$, $R_\beta = 0.43$ (see also Appendix A, Fig. 8). (Here, a, b, c and β are the MLP.)

2. Some authors have reached conclusions on the MLP changes in the pre-equiatomic composition range [9,10], where such changes are normally not expected since, in this concentration range, Ti–Ni-phase composition remains constant.
3. Temperature dependencies of Ti–Ni B19′-MLP found in [11,20,21] (in the martensitic transformation range) and in [12] (in the pure thermal expansion–contraction range) were not generally taken into consideration. [2] For example, in [10], the difference between MLP (which are determined with relatively low precision, see Table 1) for 50.0, 50.5 and 51.0 at.%Ni alloys is noted, but this conclusion, being based on the X-ray data obtained at essentially different temperatures (from +20 to −150 °C), is not valid since the influence of temperature variations on the measured parameters is not taken into account.

Also, it is unclear whether MLP are influenced by the transformation sequence (with or without an intermediate R-phase [7,14]), or by the structural and substructural state of the austenite (presence or absence of a well-developed dislocation substructure), or are affected by recovery and polygonization heat treatment [12,22]. It is also unclear whether MLP are affected by the structural and substructural state of the martensite, the latter can be either temperature-induced, reoriented, or plastically deformed [21,23]. Finally, as it can be seen from the notes to [3,11] in Table 1, the calculated MLP values depend on the number of X-ray lines used for calculations and the method of their treatment.

The aim of this work is thus to study – using identical experimental conditions, the same set of X-ray lines, and the same method of MLP calculation – the effects of nickel-concentration, temperature, strain, structural state of the parent phase and martensite on the B19′-martensite lattice parameters in binary Ti–Ni shape memory alloys. It was also interesting to compare B2-austenite and R-phase lattice parameters in alloys having different nickel-concentrations.

[2] It is stated in [4] that a temperature dependence of the MLP is absent; however, the existence of such a dependence is evident from the X-ray diffractograms presented in the same work (see also Table 1).

2. Experimental procedure

Binary Ti–Ni alloys containing 47.0, 50.0, 50.5 and 50.7 at.%Ni were studied. Their transformation temperatures after 900 °C-quenching were as follows: $M_S = 66$ °C (47.0 at.%Ni); $M_S = 68$ °C (50.0 at.%Ni); $M_S = 28$ °C, $T_R \approx 30$ °C (50.5 at.%Ni); $M_S = -20$ °C, $T_R \approx -2$ °C (50.7 at.%Ni). It must be emphasized that special attention will be further paid not only to a nominal nickel content in specific alloys, but also to their M_S temperature, the latter determined by a real nickel-concentration in solid solution [10,17–19].

Ribbon samples 0.5–1 mm thick were heated at 700 °C for 15 min, and then water-quenched. Some of the quenched Ti–50.0 at.%Ni alloy samples were deformed by rolling at room temperature (RT) with 5% or 25% of strain, which correspond, respectively, to the reorientation and plastic deformation of the martensite. Some of the 25%-strained samples were annealed at 400–430 °C for 1–2 h. Some of the quenched Ti–50.7 at.%Ni samples were aged at 450 °C for 1.5–3 h. Some of the aged Ti–50.7 at.%Ni samples were deformed by rolling at RT with 25% strain and then heated to 550 °C with a heating rate of 10°/min and quenched. Between 3 and 10 samples were used for each treatment. The 0.2 mm oxidized surface layer was removed by grinding and chemical etching from all samples.

An X-ray diffraction study was performed using an "X′ Pert Philips" diffractometer in monochromatized Cu Kα radiation. The diffractometer was equipped with special heating and cooling stages, allowing diffractograms to be obtained in the −15 to 120 °C temperature range. X-ray lines were recorded in the $2\vartheta = 36$–$84°$ range included B19′-martensite lines from (1 1 0) to (0 3 2). The precision of the camera adjustment was constantly checked, and variations in the 2ϑ angle positions of the X-ray lines of a standard quartz single crystal did not exceed ±0.01° throughout the time of the experiment.

The parameters a, b, c and β of the monoclinic B19′-martensite crystal lattice were calculated from the $2\vartheta_{hkl}$ peak positions of (1 1 0), (0 0 2), (1 1 $\bar{1}$), (0 2 0), (1 1 1), (1 1 $\bar{2}$), (0 2 2) and (0 3 2) [3] lines using the least-square method. The examples of the X-ray diffractograms of quenched Ti–50.0 and Ti–50.7 at.%Ni alloys recorded at 1 °C are presented in Fig. 1.

For the MLP calculation, the minimization of the quadratic form $\sum(2\vartheta^{exp}_{hkl} - 2\vartheta^{calc}_{hkl})^2$ was performed, where $(2\vartheta^{exp}_{hkl})$ and $(2\vartheta^{calc}_{hkl})$ are diffraction peak positions determined experimentally and from the backward MLP-based calculations. To every step of optimization, F-statistic was consistently used to test the equality of two standard deviations as referred to the measured and calculated MLP values [24]

$$F = \frac{\sum S^2_{exp}}{\sum S^2_{calc}},$$

where $S^2_{exp} = \frac{1}{n}\sum(\Delta 2\vartheta^{exp}_{hkl})^2$ is the variance of the experimental data with $\Delta 2\vartheta^{exp}_{hkl}$ representing the deviation of the experimentally measured diffraction peak positions, and $S^2_{calc} = \frac{1}{n}\sum(2\vartheta^{exp}_{hkl} - 2\vartheta^{calc}_{hkl})^2$ is the variance between experimentally measured and calculated peak positions. The F-distribution having 7 degrees of freedom for both normal populations ($7 = 8-1$ where 8 is the number of diffraction lines involved in the calculation) with a probability of 0.95 (5% significance level) was used. To find the MLP values, the steepest ascent (descent) method was employed. The calculations steps were affined, as a minimum of the quadratic function was approaching, and calculations were stopped when the last calculation path gave the F-value decrease lower than 0.01, while the optimization region was within 10^{-4}% of the calculated MLP values [24].

The precision of the MLP calculated for each set of lines is a function of the precision of the direct 2ϑ measurement, which was ±0.02–0.03° for the (1 1 0), (0 0 2), (1 1 $\bar{1}$), (0 2 0) and (1 1 1) lines; from 0.04° to 0.05° for the (1 1 $\bar{2}$) line; ~0.05° for the (0 2 2) line; and from 0.05° to 0.06°, for the (0 3 2) line.

It must be noted that the "quality" of the results depends on a number of lines involved in the calculation. In analyzing this issue, all calculations were repeated twice: firstly, the first seven lines (excluding the last one) were used, and secondly, only the first five lines were used. In both cases, after calculation, a deviation of $2\vartheta^{calc}_{hkl}$ from $2\vartheta^{exp}_{hkl}$ was verified for all eight lines measured. In the case of the seven-line calculation, a good correspondence between the calculated and measured parameters was obtained, and the value of the Fisher criterion came in under the critical threshold. For the five-line calculation, the MLP obtained by this method sometimes differ from the eight-line verification results beyond the accepted error limits. Finally for the sake of the maximum possible exactness, it was decided to use all eight measured lines for calculations.

The parameters a_R and α_R of the rhombohedral R-phase crystal lattice were calculated in an analogous fashion using the angular coordinates of the $(3\,3\,0)_R$ and $(3\,\bar{3}\,0)_R$ lines. The error limits were ±0.0002 nm and 0.05°, respectively.

The austenite lattice parameter a_{B2} was determined using the method of extrapolation to the $\vartheta = 90°$.

[3] The last line is usually referred to as (2 2 0), but the direction of its angular shift as a function of the concentration variations does not correlate with the corresponding shift of the (1 1 0) line. The indexing of this line as (0 3 2) gives minimum deviations of the calculated $2\vartheta_{hkl}$ values from the experimental ones, in all cases satisfying the Fisher criterion.

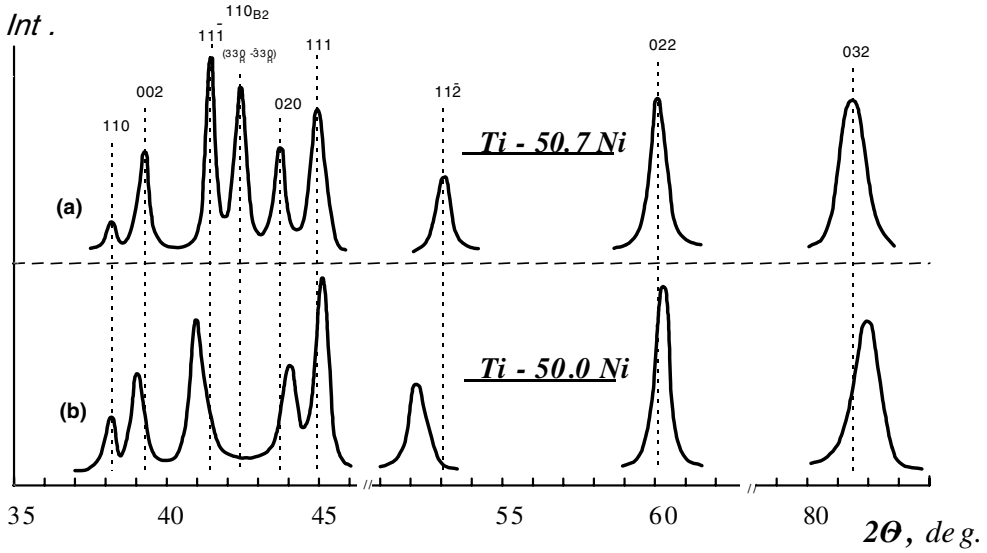

Fig. 1. X-ray diffractograms of quenched Ti–50.7 at.%Ni (a) and Ti–50.0 at.%Ni (b) alloys recorded at 1 °C: (a) after heating from −196 °C; (b) after cooling from RT.

The {1 1 0}, {2 0 0} and {2 1 1} lines and the Nelson–Riley extrapolation function were used for this calculation.

Finally, the maximum transformation lattice strain was calculated from the B19′-martensite and B2-austenite lattice parameters obtained in accordance with [25]. This strain represents a maximum relative elongation along one of the three principal strain axes when the tetragonal lattice of the austenite with the parameters $a_{B2} = a_0$, $b_{B2} = c_{B2} = a_0\sqrt{2}$ transforms into the monoclinic lattice of the martensite with parameters a, b, c and β. The procedure of calculations is based on the following considerations.

In general, when the crystal lattice is set by six parameters (three-dimensional: a, b, c and three angular: α, β, γ), the components of the metric tensor are the following:

$$\begin{Vmatrix} a^2 & a\cdot b\cdot\cos\gamma & a\cdot c\cdot\cos\beta \\ b\cdot a\cdot\cos\gamma & b^2 & b\cdot c\cdot\cos\alpha \\ c\cdot a\cdot\cos\beta & c\cdot b\cdot\cos\alpha & c^2 \end{Vmatrix}.$$

Then the tetragonal lattice of the austenite can be represented by

$$\begin{Vmatrix} a_0^2 & 0 & 0 \\ 0 & 2a_0^2 & 0 \\ 0 & 0 & 2a_0^2 \end{Vmatrix},$$

while the monoclinic lattice of the martensite, by

$$\begin{Vmatrix} a_0^2 & 0 & a\cdot c\cdot\cos\beta \\ 0 & b^2 & 0 \\ c\cdot a\cdot\cos\beta & 0 & c^2 \end{Vmatrix}.$$

The distortion tensor $\varepsilon_{ij} = \frac{1}{2}(g_{ij} - g_{ij}^0)$ can therefore be calculated, where g_{ij} and g_{ij}^0 are the components of the metric tensors of the final and initial lattices, respectively. Consequently, the matrix of the B2 → B19′ transformation strain tensor takes the following form:

$$\frac{1}{2}\begin{Vmatrix} (a^2-a_0^2)/a_0^2 & 0 & a\cdot c\cdot\cos\beta/a_0\cdot c_0 \\ 0 & (b^2-b_0^2)/b_0^2 & 0 \\ c\cdot a\cdot\cos\beta/c_0\cdot a_0 & 0 & (c^2-c_0^2)/c_0^2 \end{Vmatrix}.$$

The principal components ε_i of the transformation strain tensor, i.e., relative elongations along principal axes, can be determined from a solution of a characteristic equation obtained from the following balance:

$$\mathrm{Det}\begin{Vmatrix} (a^2-a_0^2)/2a_0^2-\varepsilon & 0 & a\cdot c\cdot\cos\beta/2a_0\cdot c_0 \\ 0 & (b^2-b_0^2)/2b_0^2-\varepsilon & 0 \\ c\cdot a\cdot\cos\beta/2c_0\cdot a_0 & 0 & (c^2-c_0^2)/2c_0^2-\varepsilon \end{Vmatrix} = 0.$$

Finally, maximum transformation strain components along principal axes are calculated as

$$\Delta L_i/L_{0i} = (1+\varepsilon_i)^{0.5} - 1.$$

Basic information for MLP calculations (angular coordinates of X-ray line peaks as functions of the nickel content and temperature) is presented in Appendix A (Figs. 9 and 10).

3. Results and discussion

3.1. Concentration dependencies of the B19′-martensite and B2-austenite lattice parameters in quenched Ti–Ni alloys

The dependencies of MLP on nickel content in quenched Ti–Ni alloys at RT are presented in Fig. 2. In the hyper-equiatomic nickel-concentration range, MLP depend on the nickel-concentration. The higher the nickel-concentration in this range, the larger the deviation from the equiatomic alloy. Corresponding deviations of X-ray lines from their "equiatomic" positions are presented in Fig. 1 for the Ti–50.7 at.%Ni alloy. Primary $2\vartheta_{hkl}$ values are given in Appendix A, Fig. 9.

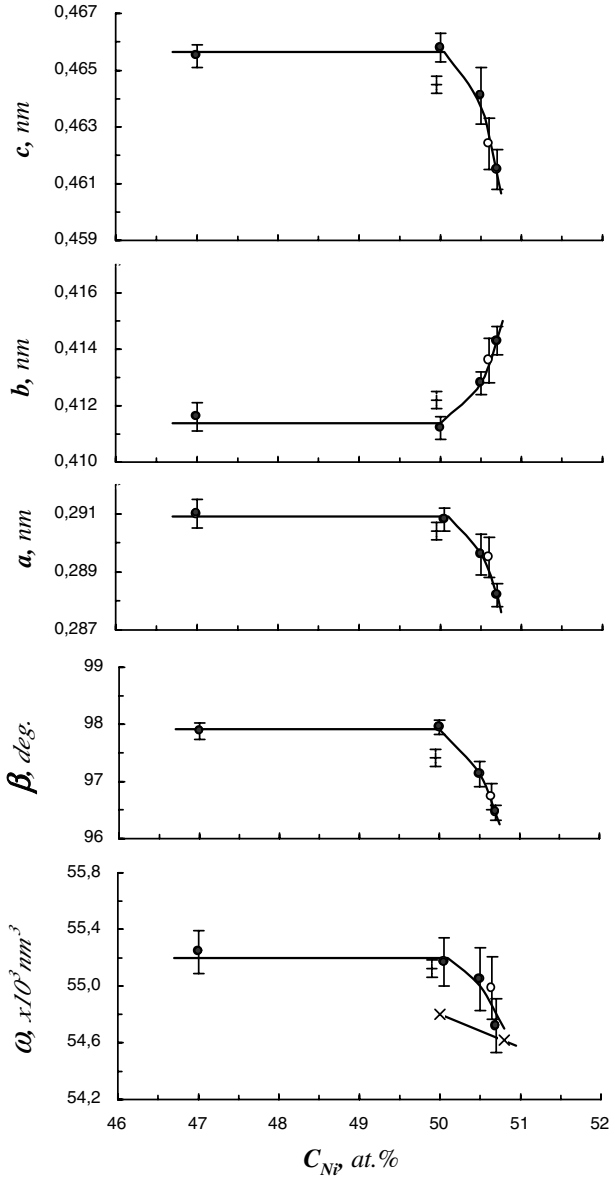

Fig. 2. Dependencies of the B19′-MLP at RT on nominal nickel content: (●) after quenching; (○) after aging at 450 °C, 1 h 20 min; (+) after 25% cold-rolling and subsequent annealing at 400 °C, 1 h; (×) doubled unit cell volume of B2-austenite.

The MLP of quenched pre-equiatomic Ti–47.0 at.%Ni and equiatomic Ti–50.0 at.%Ni alloys at RT are identical, that correlates with the constant chemical composition of the Ti–Ni-phase in this nickel-concentration range. The only difference between Ti–47 at.%Ni and Ti–50.0 at.%Ni alloys consists in the different volume fractions of the Ti_2Ni-phase.

MLP of the aged Ti–50.7 at.%Ni alloy are systematically shifted from the MLP of the quenched Ti–50.7 at.%Ni alloy towards the "equiatomic" values (see Fig. 2). That correlates with the nickel impoverishment in solid solution due to aging. For Ti–50.0 at.%Ni at RT, the unit cell volume of the B19′-martensite is higher than the doubled unit cell volume of the B2-austenite, that reflects the positive volumetric effect of the $B2 \rightarrow B19'$ transformation reported for the Ti–50.1 at.%Ni alloy [11], and for the Ti–50.5 at.%Ni alloy [26]. For the Ti–50.7 at.%Ni alloy, the difference between these parameters does not exceed calculation error limits.

The lattice parameter of the "pure" B2-austenite a_{B2} was determined for Ti–50.7 at.%Ni and Ti–50.0 at.%Ni alloys. For the Ti–50.7 at.%Ni alloy, the measurements were carried out in the 6–120 °C temperature range (quenched state) and from 24 to 120 °C (aged state). For the Ti–50.0 at.%Ni alloy, the measurements were performed at 110–120 °C. In the Ti–50.7 at.%Ni alloy, the a_{B2} amounts to 0.30121 ± 0.00007 nm at RT and to 0.30164 ± 0.00008 nm at 120 °C. In Ti–50.0 at.%Ni alloy, $a_{B2} = 0.30203 \pm 0.00008$ nm at 120 °C; extrapolation to RT leads to $a_{B2} = 0.30164 \pm 0.00006$ nm which correlates well with the a_{B2} value of 0.3015 nm, which is usually referred to as a B2-austenite lattice parameter for binary Ti–Ni alloys [27].

A decrease in the austenite unit cell volume $\omega_{B2} = a_{B2}^3$ in the hyper-equiatomic range (see Fig. 2) can be explained by an increase in nickel (having lower atomic diameter than titanium) concentration in solid solution. The martensite unit cell volume $\omega_{B19'} = abc \cdot \sin\beta$ also manifests a corresponding decrease in that range.

The a_{B2} for aged Ti–50.7 at.%Ni alloy is systematically higher than the a_{B2} for the unaged alloys because of an impoverishment of the solid solution in nickel; at RT, $a_{B2} = 0.30130 \pm 0.00009$ nm.

Finally for the sake of the validation, it is mandatory to consider not only the nominal nickel content of the alloy, but also the real nickel concentration in solid solution, which correlates with the M_S temperature position for the studied alloys (according to [10,17–19]). If one considers a dependence of the calculated MLP (using our own data as well as calculated data from Table 1) not on the nominal nickel content but on the M_S temperature, then the concentration dependence of MLP in the hyper-equiatomic range is evident (Fig. 3).

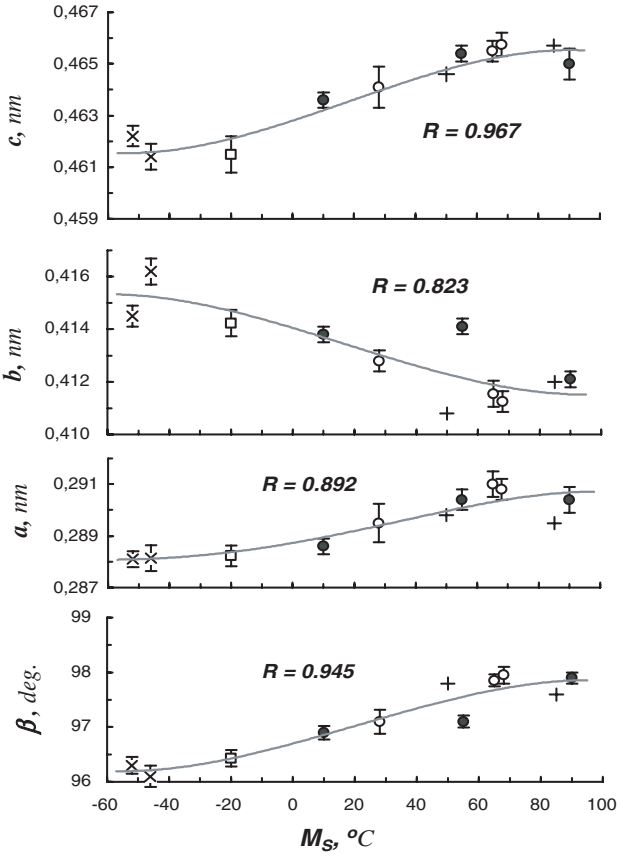

Fig. 3. Dependencies of martensite MLP at RT on the M_S temperature position: (○, □) present investigation; (●, ×) calculated using d_{hkl} or ϑ_{hkl} data from [2,4,11,12,15] (see Table 1); (□, ×) extrapolated to RT from lower-temperatures; (+) taken from [9,14]. R, are the correlation coefficients.

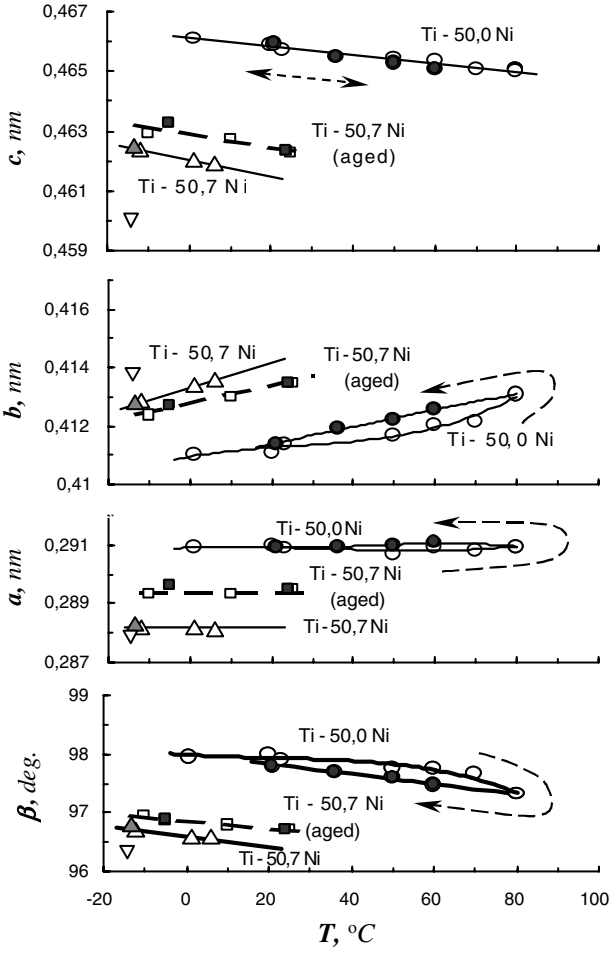

Fig. 4. Temperature dependencies of B19′-MLP: (○, ●) Ti–50.0 at.%Ni, after quenching at 1 °C; △, ▲ Ti–50.7 at.%Ni, after quenching at −196 °C; (□, ■) Ti–50.7 at.%Ni, after quenching and aging at 450 °C, 1 h 20 min and subsequent cooling down to −196 °C; (▽) Ti–50.7 at.%Ni, after quenching, aging, cold rolling, annealing at 550 °C, cooling to −196 °C and reheating to −15 °C; (○, △, □, ▽), heating; (●, ▲, ■), cooling.

An increase in real nickel-concentration with a decrease in M_S is also confirmed by the simultaneous lowering in the martensite unit cell volume: from 55.2×10^{-3} nm^3 at $M_S \approx 80$ °C to 54.8×10^{-3} nm^3 at $M_S = -50$ °C (from the data of Fig. 3).

Note also that the MLP of the martensite formed from the austenite containing a well-developed dislocation substructure (resulted from 25% cold-rolling and partial recovery heat treatment at 400–430 °C for Ti–50.0 at.%Ni alloy or polygonizing heat treatment at 550 °C for Ti–50.7 at.%Ni alloy – see [28]) deviate from the corresponding MLP of the quenched martensite formed from a low-dislocated recrystallized austenite (see Figs. 2, 4 and 6).

3.2. Calculation of the maximum B19′ → B2 transformation strain

Knowing the maximum B2 → B19′ transformation lattice strain is important from a practical point of view, because it determines the maximum fully recoverable strain obtained from the material. A maximum transformation strain for the quenched Ti–50.0 at.%Ni and Ti–50.7 at.%Ni alloys was calculated for the two different temperatures: (a) using B2 and B19′ lattice parameters near the M_S temperature of each alloy, and (b) using the lattice parameters referred to RT. The results of the calculations are presented in Table 2, and show that the maximum transformation strain, and consequently the theoretical resource of the maximum recovery strain in the Ti–50.0 at.%Ni alloy (12.07 at RT), is from 11% to 17% higher than in the Ti–50.7 at.%Ni alloy (10.31 at RT).

3.3. Temperature dependencies of the B19′-martensite lattice parameters

3.3.1. General remarks

Temperature dependencies of MLP are observed in the investigated nickel concentration range and they are

approximately the same for different alloys (including the aged Ti–50.7 at.%Ni alloy): for each alloy, in the range of the martensite existence, the difference between MLP measured at various temperatures remains approximately constant (Fig. 4).

The resulting volume expansion of the martensite lattice is observed upon heating (see Fig. 4). However, if the lattice changes are considered in terms of thermal expansion coefficients (TEC), then, as can be concluded from the $2\vartheta_{hkl}$ variations (see Appendix A, Fig. 10), TEC is positive for the directions normal to the (1 1 0), (0 2 0), (1 1 1), (0 2 2) and (0 3 2) planes, while being negative for the (1 1 $\bar{1}$), (1 1 $\bar{2}$) and, under certain conditions, for the (0 0 2) planes.

The same shifts of $2\vartheta_{hkl}$ coordinates caused by temperature variations were noted for the (0 0 2), (1 1 $\bar{1}$), (0 2 0) and (1 1 1) lines in [12], for the (1 1 0), (1 1 1), (1 1 $\bar{2}$) and (0 3 2) lines in [22,23], and could be also observed on the diffractograms presented in [4] – (1 1 0), (1 1 1), (0 2 0) and (1 1 1) lines, [11] – (1 1 0), (1 1 $\bar{1}$), (0 2 0) and (1 1 1) lines, and finally, [20] – (1 1 $\bar{1}$), (0 2 0) and (1 1 1) lines.

The negativity of the TEC in the direction normal to the (0 0 2) plane (which was also found for the Ti–50.5 at.%Ni alloy in [12]), is not very obvious for the quenched pre-equiatomic and equiatomic alloys (as also in [11]). It would be more prudent to conclude here that the TEC in these alloys is close to zero within small error limits (see Appendix A, Fig. 10). However, for the Ti–50.7 at.%Ni alloy, the TEC is evidently negative (see Appendix A, Fig. 10).

The transformation sequence in alloys with different nickel content is not the same. At RT, the structure of the as-quenched Ti–50.0 at.%Ni alloy is fully martensitic (without considering a small quantity of the Ti_2Ni-phase, which is present in all studied alloys, but to a different extent). Changes in MLP in the temperature range below the starting point of the reverse transformation are fully reversible. During heating of the Ti–50.0 at.%Ni (as well as Ti–47.0 at.%Ni) alloy in the 70–80 °C range, the B19′-martensite partially transforms into austenite (see Fig. 5(a); note that in this particular experiment, the pure austenitic state was not reached, and that at 80 °C, the material contained about 25–30% of the retained martensite). Upon subsequent cooling, first, at 60 °C, the austenite starts the direct transformation to martensite, then just above 40 °C, the transformation passes through an intermediate R-phase, and at 40 °C and lower, only the B19′ and R-phases coexist. Finally at 30 °C, the R-phase completely transforms to the B19′ phase (see Fig. 5(a)). The Ti–47.0 at.%Ni alloy differs from the Ti–50.0 at.%Ni alloy in a somewhat higher fraction of the Ti_2Ni-phase and in presence of ≈5% of the retained austenite after quenching, but the structural changes in heating–cooling cycles are analogous.

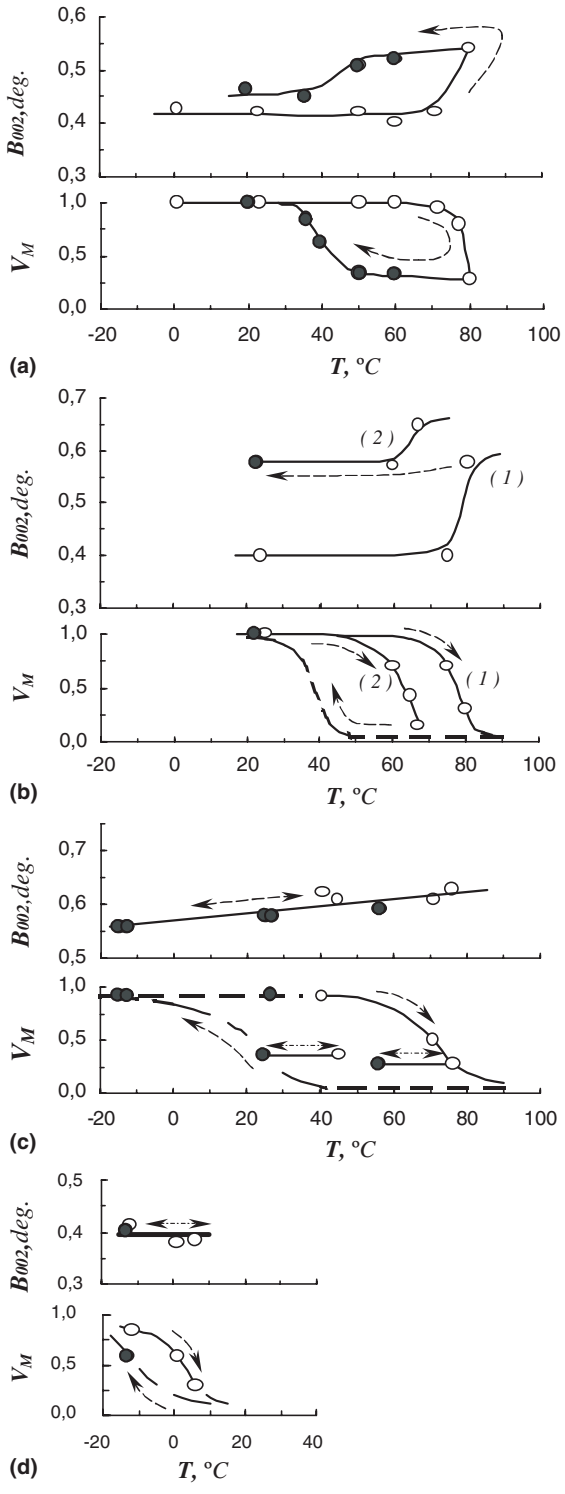

Fig. 5. Temperature dependencies of the B19′ (0 0 2) line half-width and martensite volume fraction: (a)–(c), Ti–50.0 at.%Ni alloy: (a) after quenching; (b(1)) after quenching, (b(2)) after a cycle of the complete reverse-direct transformation; (c) after cold plastic deformation and partial recovery at 400 °C; (d) Ti–50.7 at.%Ni after quenching; light symbols – cooling; dark symbols – heating.

It seems that the partial reverse martensitic transformation (RMT) in the 70–80 °C range for the Ti–50.0 at.%Ni alloy enhance the MLP temperature dependen-

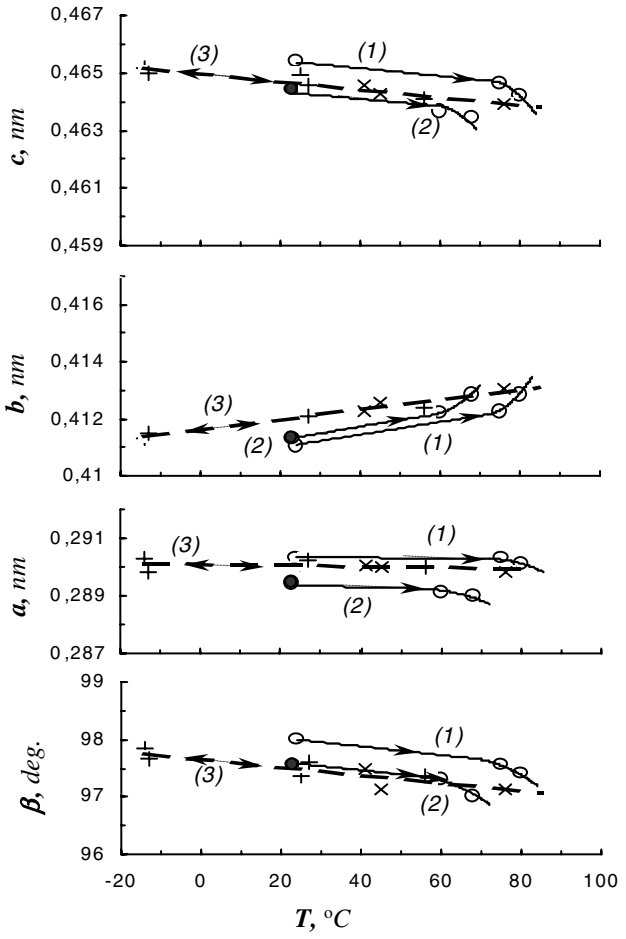

Fig. 6. Temperature dependencies of the B19′-MLP for the Ti–50.0 at.%Ni alloy: (1) after quenching; (2) after one complete cycle reverse-direct transformation (transformation-induced hardening); (3) after cold plastic deformation with partial recovery at 400 °C. (○, ×) heating; (●, +) cooling.

cies (see Fig. 4). Temperature dependencies of the $2\vartheta_{hkl}$ which are determined with higher precision than the calculated MLP, demonstrate this phenomenon more clearly (see Appendix A, Fig. 10). For the Ti–50.7 at.%Ni alloy, this effect is not observed (see Fig. 4).

At RT, while Ti–50.5 at.%Ni alloy contains almost exclusively R-phase and B19′-martensite, quenched Ti–50.7 at.%Ni alloy is fully austenitic. During cooling of the Ti–50.7 at.%Ni alloy, the R-phase appears at −2 °C, and partially transforms to the B19′-martensite in the −10 to −35 °C temperature range (see Fig. 5(d)) (≈10% of the R-phase still remains after cooling down to even −196 °C). During subsequent heating, in the −5 to 12 °C range, the martensite transforms to the B2-austenite through an intermediate R-phase; incidentally B19′ → R and R → B2 transformations overlap (which follows from diffractograms as well as from an independent DSC study).

At RT, the structure of the aged Ti–50.7 at.%Ni alloy represents a mixture of 60% R-phase and 40% B2-austenite. During cooling, the austenite transforms to the martensite through the R-phase. This process finishes somewhat below −15 °C. RMT in aged alloys proceeds through the same transformation sequence as in as-quenched alloys, but at higher-temperatures (between 10 and 35 °C) because of the impoverishment of a solid solution in nickel due to aging.

3.3.2. Influence of the austenite dislocation substructure on the MLP temperature dependencies

At RT, the structure of the Ti–50.0 at.%Ni alloy first cold-deformed and then partially recovered at 400 °C consists of B19′ and R-phases in approximately equal fractions (Fig. 5(c)). In this case, the existence of the well-developed dislocation substructure in the austenite promotes R-transformation and lowers the temperatures of the martensite formation and reverse transformation [27]. Upon cooling, in the 40 to −10 °C range, the R-phase transforms to martensite (≈10% of R-phase remains untransformed). Upon heating, in the 50–80 °C range, the martensite transforms back to the B2-austenite through the R-phase (see Fig. 5(c)).

The MLP of the martensite formed in the Ti–50.0 at.%Ni alloy from the austenite containing a well-developed dislocation substructure differ from the MLP of the as-quenched martensite; their temperature dependencies are preserved (see Fig. 6). In the cases presented in Fig. 6, the austenite was strengthened by transformation-induced hardening resulting from a completed RMT or by partially preserved strain-induced hardening caused by cold-rolling and partial recovery annealing at 400–430 °C. Note that in this case, the TEC in the direction normal to the (0 0 2) plane is obviously negative as also demonstrated in [12].

The enhancement of the MLP temperature dependencies in the course of the RMT of quenched martensite is also visible (see Fig. 6). In this case, the RMT of quenched martensite during the first heating was completed (unlike with the incomplete RMT presented in Fig. 4). Obviously, transformation-induced hardening caused by the completed RMT is higher than that due to the partial RMT. It causes bigger changes in the MLP after cooling (compare Figs. 4 and 6), and subsequently, upon second heating, the MLP of the initially quenched martensite become comparable to the MLP of the martensite formed from the partially recovered austenite (see Fig. 6).

This explanation of the MLP temperature dependencies, based on the increase in dislocation density due to transformation or strain-induced hardening, is proven by an increase in the (0 0 2) X-ray line half-width, which, for Ti–50.0 at.%Ni alloys, turned out to be 1.5 times higher than for the as-quenched condition (see Fig. 5(b) and (c)).

For the same Ti–50.0 at.%Ni alloy, in the case of the initially hardened austenite, the X-ray line width increases only slightly during RMT. What is more, in the quenched or aged Ti–50.7 at.%Ni alloy, no changes in X-ray line width were observed during RMT. It can be concluded that in both cases, transformation-induced hardening is not pronounced and does not influence the temperature dependencies of MLP (see Fig. 5(c) and (d)). In the first case, the accumulation of the transformation-induced hardening is prevented by the initial substructural hardening, and in both cases, this hardening is avoided by the presence of an intermediate R-phase, which offers a better lattice accommodation for transformation than a direct $B19' \rightarrow B2$ sequence.

It must be borne in mind that the calculated MLP can be affected not only by stresses from the dislocation substructure, but also by interphase stresses appearing in the course of the martensitic transformation, [4] as well as by residual stresses of various origins. The data presented in [12] indicate such a possibility, which requires special examination.

3.3.3. On the influence of an intermediate R-phase on the MLP temperature dependencies

It is important here to specify the role of the structural state of the material on the MLP. Based on the observed in [7,14] differences in the MLP of binary Ti–Ni alloys of different compositions, it was first supposed that these differences are related to different phases, from which the martensite originates. Indeed, on the one hand, the R-phase is the parent phase for the martensite in alloys with hyper-equiatomic nickel-concentration or with highly dislocated austenite. On the other hand, for the martensite formed in quenched Ti–47.0 at.%Ni and Ti–50.0 at.%Ni alloys, the parent phase is B2-austenite.

However, as it is seen from Fig. 4 for the Ti–50.0 at.%Ni alloy, the transition, at 40 °C, from the $B2 \rightarrow B19'$ to $B2 \rightarrow R \rightarrow B19'$ transformation sequence does not provoke "backward" changes in the MLP temperature dependencies. On the contrary, even in the case when the martensite forms from the R-phase in all cases (Ti–50.7 at.%Ni alloy), the MLP were found different for recrystallized (quenched), aged and highly dislocated (partially recovered) initial austenites (Fig. 4). It could therefore, be concluded, that changes in MLP for the B19′-martensite in hyper-equiatomic alloys, or in alloys with hardened austenite, compared to quenched equiatomic alloys, are not affected in any way by the

Table 2
Calculated maximum transformation lattice strain of $B2 \rightarrow B19'$ transformation in quenched Ti–50.0% Ni and Ti–50.7% Ni alloys

Alloy	Near M_s (at 50 °C for Ti–50.0 at.%Ni and at −12 °C for Ti–50.7 at.%Ni)						At RT					
	a_{B2} (nm)	a (nm)	b (nm)	c (nm)	β (°)	ε_{max} (%)	a_{B2} (nm)	a (nm)	b (nm)	c (nm)	β (°)	ε_{max} (%)
50.0% Ni	0.30175	0.29100	0.41230	0.46540	97.80 ± 0.10	11.92 ± 0.26	0.30164	0.29090	0.41135	0.46570	97.90 ± 0.10	12.07 ± 0.25
	±0.00007	±0.00030	±0.00035	±0.00035			±0.00006	±0.00030	±0.00035	±0.00035		
50.7% Ni	0.30107	0.28820	0.41280	0.46230	96.70 ± 0.15	10.74 ± 0.35	0.30121	0.28820	0.41430	0.46140	96.35 ± 0.15	10.31 ± 0.35
	±0.00007	±0.00040	±0.00050	±0.00060			±0.00007	±0.00040	±0.00050	±0.00060		

[4] The interphase stresses contribute to the X-ray line width, which increases in the course of the RMT, especially in its final stage when martensite crystals undergo elastic interaction with the surrounding austenite (see Fig. 5(b) and (c)).

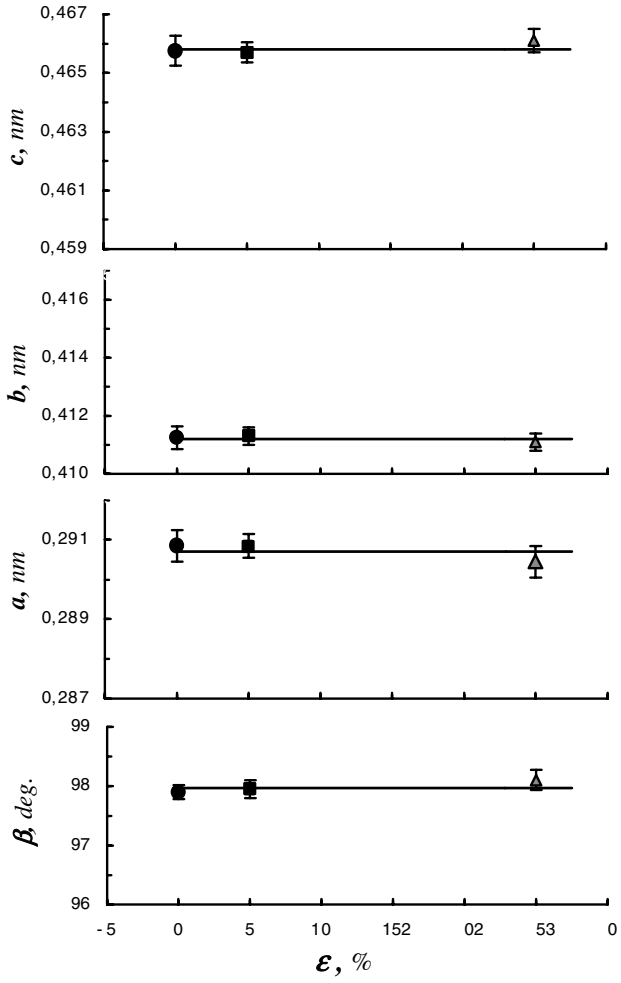

Fig. 7. Lattice parameters of quenched, reoriented ($\varepsilon = 5\%$) and plastically deformed ($\varepsilon = 25\%$) martensites in Ti–50.0 at.%Ni alloy.

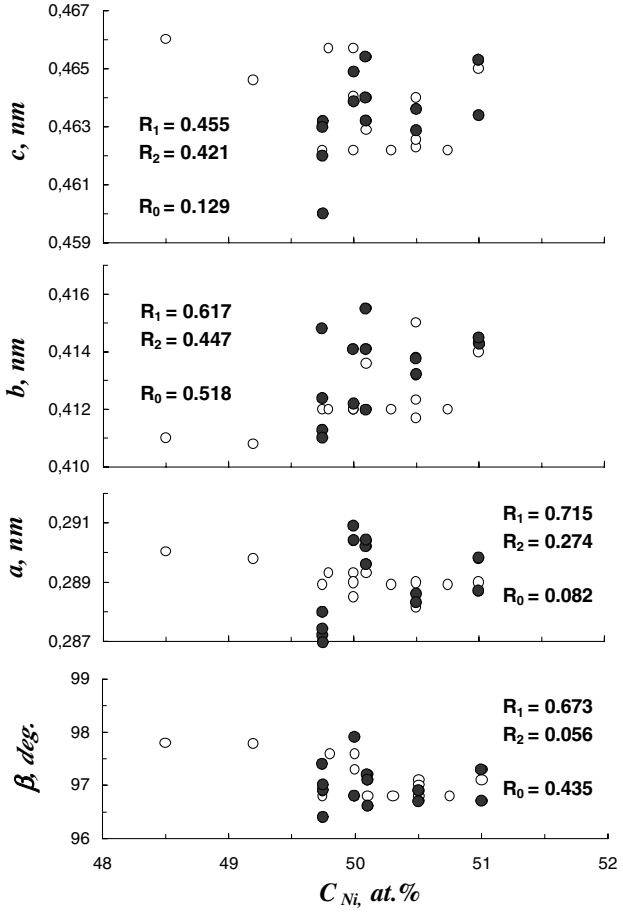

Fig. 8. To the evaluation of the correlation coefficient between MLP of B19′-martensite and nominal nickel content in binary Ti–Ni alloys taken from different sources (see Table 1); R_1 directly given reference MLP (○); R_2 MLP calculated from the ϑ_{hkl} or d_{hkl} taken from different sources (●); R_0 combined results.

Table 3
R-phase lattice parameters in Ti–Ni alloys

Alloy, treatment	Recoding temperature (°C)	Retained R-phase fraction (%)	a_R (nm)	α_R (°)
Ti–50.7 at.%Ni, quenching + reheating from −196 °C	−12	10–15	0.3012 ± 0.0002	89.28 ± 0.05
Ti–50.7 at.%Ni, quenching + aging + reheating from −196 °C	−15	10–15	0.3014 ± 0.0002	89.20 ± 0.05
Ti–50.0 at.%Ni, quenching + OMT + cooling	36	~15	0.3021 ± 0.0002	89.49 ± 0.05
Ti–50.0 at.%Ni, CW($\varepsilon = 25\%$) + 400° + reheating from −196 ° C	RT	~20	0.3017 ± 0.0002	89.27 ± 0.05
Ti–50.7 at.%Ni, quenching + cooling	−15	~40	0.3012 ± 0.0002	89.45 ± 0.05
Ti–50.7 at.%Ni, quenching + aging + cooling	0	70–75	0.3014 ± 0.0002	89.30 ± 0.05
Ti–50.5 at.%Ni, quenching	RT	80	0.3015 ± 0.0002	89.53 ± 0.05
Ti–50.0 at.%Ni, CW ($\varepsilon = 25\%$) + 400 °C	RT	~70	0.3017 ± 0.0002	89.36 ± 0.05

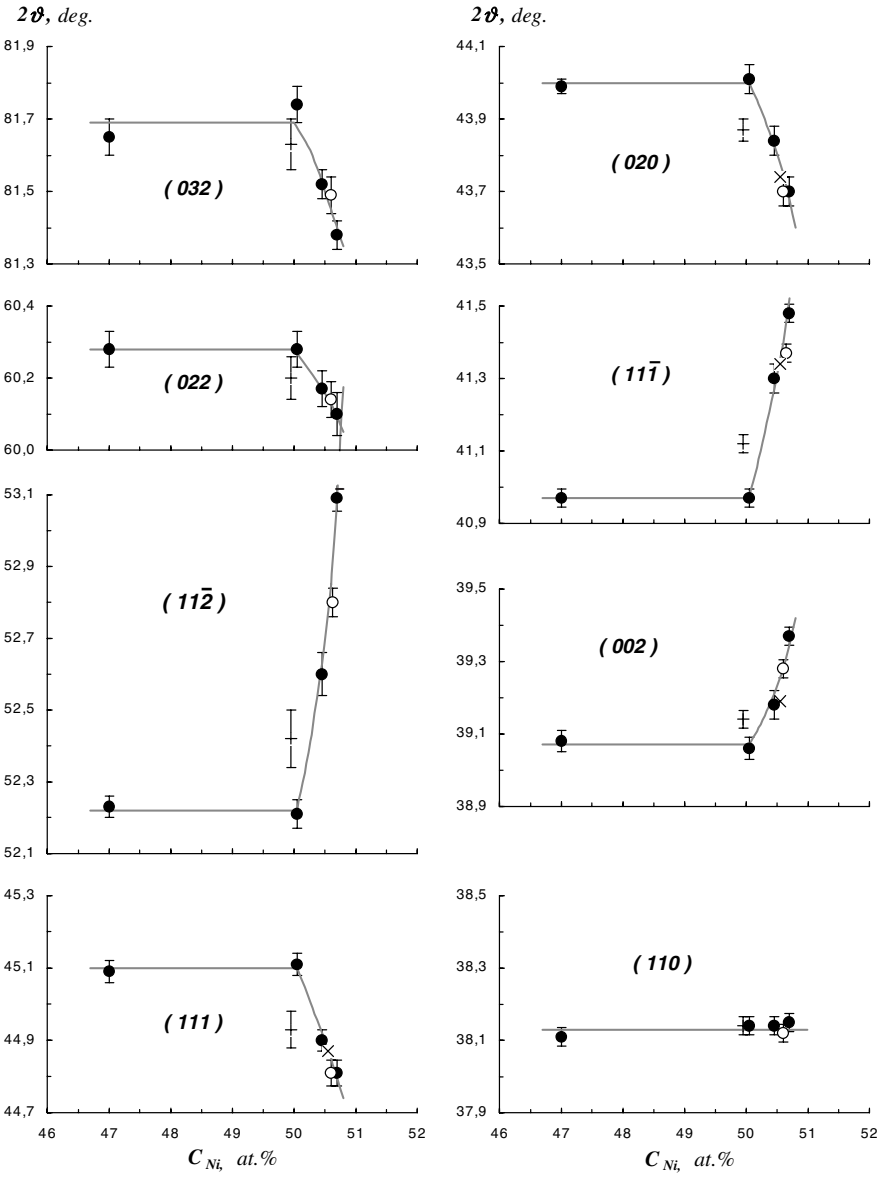

Fig. 9. Dependencies of $2\vartheta_{hkl}$ coordinates of B19′-martensite on nominal nickel content at RT: (●) after quenching; (○) after aging at 450 °C, 1 h 20 min; (+) after 25% cold-deformation at RT and subsequent annealing at 400 °C, 1 h; (×) data for the quenched Ti–50.5 at.%Ni [12].

presence of the R-phase, but rather by the structural state of the material.

3.4. Lattice parameters of the deformed martensite

At RT, the MLP of either quenched, reoriented ($\varepsilon = 5\%$), or plastically deformed ($\varepsilon = 25\%$) martensites in the Ti–50.0 at.%Ni alloy are identical (see Fig. 7). Evidently, an additional "mechanical" action on the martensite during its formation (due to the presence of the well-developed dislocation substructure in the transformation- or strain-hardened austenite) modifies the MLP, as shown in Figs. 2, 4 and 6. But if this mechanical action is applied to the already formed martensite, the MLP are not affected.

3.5. Lattice parameters of the R-phase

Since the rhombohedral distortion of the R-phase lattice continuously increases upon cooling below T_R, and stabilizes by the end of the $R \rightarrow B19'$ transformation only [11], it is reasonable to compare R-phase lattice parameters in the same structural state, i.e., either at the final phase of the $R \rightarrow B19'$ transformation, or at the same fraction of the R-phase transformed to the martensite. The results of corresponding calculations are

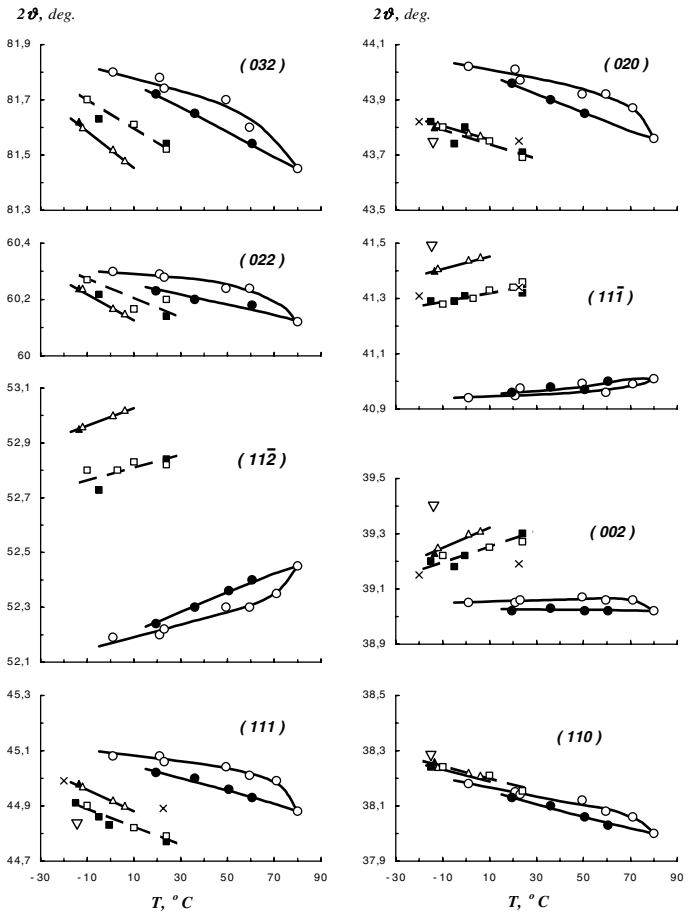

Fig. 10. Temperature dependencies of $2\vartheta_{hkl}$ coordinates of B19′-martensite: (○, ●) Ti–50.0 at.%Ni, after quenching at 1 °C; (△, ▲) Ti–50.7 at.%Ni, after quenching at −196 °C; (□, ■) Ti–50.7 at.%Ni, after quenching and aging at 450 °C, 1 h 20 min and cooling down to −196 °C; (○, △, □, ▽) heating; (●, ▲, ■) cooling; (▽) Ti–50.7 at.%Ni, after quenching, aging, cold rolling, annealing at 550 °C, cooling to −196 °C and reheating to −15 °C; (×) data for the quenched Ti–50.5 at.%Ni [12].

presented in Table 3. It can be observed that the higher the nickel-concentration, the higher the rhombohedral distortion of the R-phase lattice. The same trend is observed when the additional factors promoting R-phase formation are present (aging or strain- or transformation-induced hardening).

4. Conclusions

1. In the hyper-equiatomic nickel-concentration range of binary Ti–Ni alloys, concentration dependencies of the lattice parameters of the quenched B19′-martensite are observed. The parameters a, c, β decrease, while b increases as nickel-concentration increases. The martensite unit cell volume $\omega_{B19'}$ incidentally decreases in accordance with a decrease in the B2-austenite unit cell volume ω_{B2}, that is a direct result of a solid solution enrichment in nickel. In the pre-equiatomic nickel-concentration range, the B19′-martensite lattice parameters do not change.
2. For Ti–50.0 at.%Ni alloy, maximum martensitic transformation lattice strain and, consequently, theoretical resource of the maximum fully recoverable strain is from 11% to 17% higher than for Ti–50.7 at.%Ni alloys.
3. Lattice parameters of the B19′-martensite formed from the austenite containing a well-developed dislocation substructure (caused either by partial recovery after cold working or by transformation-induced hardening) differ from the lattice parameters of the quenched B19′-martensite.
4. For binary Ti–Ni, temperature dependencies of the B19′-MLP are observed. These trends are approximately the same in the entire 47.0–50.7 at.%Ni concentration range: as temperature increases, parameter a slightly varies, b increases, and c and β decrease. The unit cell volume increases during heating, thus reflecting a thermal volume expansion of the B19′-martensite lattice. For quenched Ti–47 at.%Ni and Ti–50.0 at.%Ni alloys, an enhancement of the temperature dependencies of the MLP occurs in the

course of the RMT. Such enhancement is absent when the martensite is formed in the Ti–50.7 at.%Ni alloy from quenched austenite and in the Ti–50.0 at.%Ni and Ti–50.7 at.%Ni alloys, from the austenite containing well-developed dislocation substructure. In the latter cases, an additional transformation-induced hardening is prevented because of the strong preliminary strain-induced hardening of the austenite, or because the transformation itself occurs through an intermediate R-phase (good accommodation of lattices during transformation).

5. The change in the transformation sequence from $B2 \rightarrow B19'$ to $B2 \rightarrow R \rightarrow B19'$ is not a cause for changes in the B19′-MLP connected to the nickel concentration variations, or to the effect of strain- or transformation-induced hardening of the B2-austenite.
6. For the Ti–50.0 at.%Ni alloy, reorientation or plastic deformation (25% of thickness reduction) of the B19′-martensite do not affect its MLP.
7. An increase in rhombohedral distortion of the R-phase lattice with the increase in the nickel-concentration in solid solution is observed. The same effect can also be initiated by other factors promoting R-phase formation (aging and strain or transformation-induced hardening of the austenite).

Acknowledgements

This work had been carried out with partial support from the Russian Foundation for Basic Research (Grant No. 00-15-99083) and from the Natural Science and Engineering Research Council of Canada. The authors recognize Jacques Desrochers for his technical assistance.

Appendix A

In the Appendix, the primary X-ray diffraction data ($2\vartheta_{hkl}$ angles) used for the correlation analysis of MLP dependencies on a nominal nickel content (Fig. 8), as well as for the MLP calculations (Figs. 9 and 10) are presented. Fig. 9 corresponds to Fig. 2 and Fig. 10 to 4 of the article.

References

[1] Dautovich DP. Can Met Quart 1965;4:129.
[2] De Lange RG, Ziderveld JA. J Appl Phys 1968;39:2195.
[3] Otsuka K, Sawamura T, Shimizu K. Phys Status Solidi (a) 1971;5:457.
[4] Otsuka K, Sawamura T, Shimizu K, Wayman CM. Metal Trans 1971;2:2583.
[5] Hehemann RF, Sandrock GD. Scripta Met 1971;5:801.
[6] Tadaki T, Wayman CM. Scripta Met 1980;14:801.
[7] Monasevich LA, Paskal YuI. Fiz Met Metalloved 1980;49:813 [in Russian].
[8] Michal GM, Sinclair R. Acta Cryst 1981;B37:1803.
[9] Kudoh Y, Tokonami M, Miyazaki S, Otsuka K. Acta Met 1985;33:2049.
[10] Khachin VN, Pushin VG, Kondratyev VV. Titanium nickelide: structure and properties. Moscow; 1992. p. 178 [in Russian].
[11] Mironov YP, Kulkov SN. Izvestya VUZov Fizika 1994;8:49 [in Russian].
[12] Gundyrev VM, Zel'dovich VI, Sobyanina GA. Textures Microstruct 1999;32:71.
[13] Pushin VG, Kondratyev VV, Khachin VN. Pretransformation phenomena and martensitic transformations. Ekaterinburg; 1998. p. 368 [in Russian].
[14] Monasevich LA, Borisova SD, Paskal YuL. Crystallogeometry of structural phase transitions in titanium nickelide. Izvestya VUZov Fizika, Deposed article, Tomsk; 1979. p. 33 [in Russian].
[15] Savvinov AS, Sivokha VP, Voronin VP, Khachin VN. Structure transition in titanium–nickelide-based alloys. Izvestya VUZov Fizika, Deposed article, Tomsk; 1984. p. 17 [in Russian].
[16] Lukass P, Sittner P, Neov D, Novak V, Ludovyy D, Tovar M. Mater Sci Forum 2002;404–407:835.
[17] Grishkov VN, Lotkov AI. Fiz Met Metalloved 1985;60:351 [in Russian].
[18] Melton KN. Ni–Ti based shape memory alloys. In: Duerig TW, et al, editors. Engineering aspects of shape memory alloys. London; 1990. p. 21.
[19] Khalil-Allafi J, Dlouhy A, Eggeler G. Acta Mater 2002;50:4255, 17.
[20] Bondareva SA. PhD thesis. Moscow; 1992. p. 142 [in Russian].
[21] Prokoshkin SD, Turenne S, Khmelevskaya IYu, Brailovski V, Trochu F. Can Met Quart 2000;39:225.
[22] Turenne S, Prokoshkin SD, Brailovski V, Sacepe N. Can Met Quart 2000;39:217.
[23] Prokoshkin SD, Turenne S, Khmelevskaya IYu, Brailovski V, Trochu F. Phys Met Metallogr 2000;90:128.
[24] Montgomery DC. Design and analysis of experiments. New York: Wiley; 1983.
[25] Shape memory alloys and their applications in medicine. In: Monasevich LA, editor. Novosibirsk; 1992. p. 742 [in Russian].
[26] Gundyrev VM, Zeldovich VI. Fiz Met Metalloved 2001;91:104 [in Russian].
[27] Otsuka K, Wayman CM, editors. Shape memory materials. Cambridge; 1998. p. 284.
[28] Prokoshkin SD, Khmelevskaya IYu, Brailovski V, Trochu F, Turenne S, Turilina VYu. Can Met Quart 2004;43:95.